

Accepted Manuscript

Predicting the drying properties of sludge based on hydrothermal treatment under subcritical conditions

Mikko Mäkelä, Laurent Fraikin, Angélique Léonard, Verónica Benavente, Andrés Fullana



PII: S0043-1354(15)30441-3

DOI: [10.1016/j.watres.2015.12.043](https://doi.org/10.1016/j.watres.2015.12.043)

Reference: WR 11741

To appear in: *Water Research*

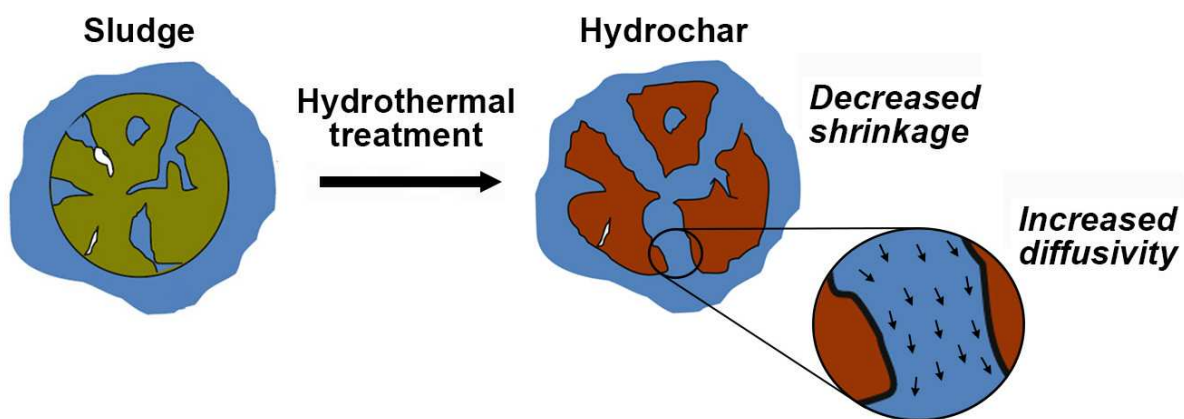
Received Date: 2 September 2015

Revised Date: 15 December 2015

Accepted Date: 24 December 2015

Please cite this article as: Mäkelä, M., Fraikin, L., Léonard, A., Benavente, V., Fullana, A., Predicting the drying properties of sludge based on hydrothermal treatment under subcritical conditions, *Water Research* (2016), doi: 10.1016/j.watres.2015.12.043.

This is a PDF file of an unedited manuscript that has been accepted for publication. As a service to our customers we are providing this early version of the manuscript. The manuscript will undergo copyediting, typesetting, and review of the resulting proof before it is published in its final form. Please note that during the production process errors may be discovered which could affect the content, and all legal disclaimers that apply to the journal pertain.



1 **Predicting the drying properties of sludge based on hydrothermal**
2 **treatment under subcritical conditions**

3 Mikko Mäkelä^{*a}, Laurent Fraikin^b, Angélique Léonard^b, Verónica Benavente^c, Andrés Fullana^c

4 ^a Swedish University of Agricultural Sciences, Department of Forest Biomaterials and Technology,
5 Skogsmarksgränd, 90183 Umeå, Sweden

6 *Current address: Tokyo Institute of Technology, Department of Environmental Science and*
7 *Technology, G5-8, 4259 Nagatsuta-cho, Midori-ku, Yokohama 226-8502, Japan*

8 ^b University of Liège, Department of Chemical Engineering, Agora, B6c, Allée du 6 Août, 4000
9 Liège, Belgium (L. Fraikin: laurent.fraikin@ulg.ac.be, A. Léonard: a.leonard@ulg.ac.be)

10 ^c University of Alicante, Department of Chemical Engineering, P.O. Box 99, 03080 Alicante, Spain
11 (V. Benavente: veronica.benavente@ua.es, A. Fullana: andres.fullana@ua.es)

12 ^{*}corresponding author, tel.: +81 (0)45 924 5507, fax: +81 (0)45 924 5507, email:
13 makela.m.aa@m.titech.ac.jp, mikko.makela@slu.se

14

15 **Abstract**

16 The effects of hydrothermal treatment on the drying properties of sludge were determined. Sludge
17 was hydrothermally treated at 180-260 °C for 0.5-5 h using NaOH and HCl as additives to influence
18 reaction conditions. Untreated sludge and attained hydrochar samples were then dried under identical
19 conditions with a laboratory microdryer and an X-ray microtomograph was used to follow changes in
20 sample dimensions. The effective moisture diffusivities of sludge and hydrochar samples were
21 determined and the effect of process conditions on respective mean diffusivities evaluated using
22 multiple linear regression. Based on the results the drying time of untreated sludge decreased from
23 approximately 80 minutes to 37-59 minutes for sludge hydrochar. Drying of untreated sludge was
24 governed by the falling rate period where drying flux decreased continuously as a function of sludge
25 moisture content due to heat and mass transfer limitations and sample shrinkage. Hydrothermal
26 treatment increased the drying flux of sludge hydrochar and decreased the effect of internal heat and
27 mass transfer limitations and sample shrinkage especially at higher treatment temperatures. The
28 determined effective moisture diffusivities of sludge and hydrochar increased as a function of
29 decreasing moisture content and the mean diffusivity of untreated sludge ($8.56 \cdot 10^{-9} \text{ m}^2 \text{ s}^{-1}$) and
30 sludge hydrochar ($12.7\text{-}27.5 \cdot 10^{-9} \text{ m}^2 \text{ s}^{-1}$) were found statistically different. The attained regression
31 model indicated that treatment temperature governed the mean diffusivity of hydrochar, as the effects
32 of NaOH and HCl were statistically insignificant. The attained results enabled prediction of sludge
33 drying properties through mean moisture diffusivity based on hydrothermal treatment conditions.

34 **Keywords:** Biosolids; Moisture diffusivity; Hydrochar; Hydrothermal carbonization; Shrinkage; X-
35 ray microtomography

36 1. Introduction

37 Handling of sludge residues generated by biological and chemical wastewater treatment processes is
38 becoming ever more challenging due to rapid urbanization and increasing efficiency requirements for
39 municipal and industrial wastewater treatment plants. Sludge residues are widely complex materials
40 due to a variety of structural components such as extracellular polymeric structures, filamentous
41 bacteria, cationic salts and the potential presence of pollutant precursors, e.g., proteins and fats,
42 pathogens, parasites, trace metals, polychlorinated biphenyls, dioxins and other slowly decomposable
43 compounds (Vaxelaire and Cézac, 2004; Yoshikawa and Prawisudha, 2014b). Currently the most
44 common sludge handling methods include incineration, composting, use in agriculture or disposal in
45 landfills (Mahmood and Elliott, 2006; Mowla et al., 2013), although current trends in European
46 regulation are increasingly hindering landfill deposition of organic substances. As sludge is an
47 inherently wet material decreasing associated handling, storage and transportation costs generally
48 requires active drying especially for smaller-scale treatment plants. However current means of
49 mechanical dewatering suffer from difficulties in removing intracellular and chemically bound water
50 from the polymeric matrix of sludge suspensions (Mowla et al., 2013; Stoica et al., 2009).

51 Hydrothermal treatment performed with water acting as a solvent, a reactant and even a catalyst or
52 catalyst precursor does not require prior drying of a sludge feedstock and allows simultaneous
53 elimination of biologically active organisms or compounds (Peterson et al., 2008). Hydrothermal
54 treatment under subcritical conditions can be used for producing carbonaceous hydrochar with
55 relatively high yields (Libra et al., 2011) and enables the conversion of non-traditional feedstock such
56 as municipal and industrial sludge residues. The increasing ion product of water under hydrothermal
57 conditions typically favours reactions which are catalyzed by acids or bases and is generally
58 understood to proceed via a network of hydrolysis, dehydration, decarboxylation, polymerization and
59 aromatization of biomass components (Kruse et al., 2013; Sevilla and Fuertes, 2009). As
60 hydrothermal treatment is ideally operated under saturated steam pressure the latent heat requirement
61 of evaporation can also be avoided although post-separation of solid and liquid phases is still required.
62 Irrespective of potential hydrochar applications such as direct solid fuel replacement, soil

63 amelioration or metal/metalloid adsorption (Alatalo et al., 2013; Libra et al., 2011; Titirici and
64 Antonietti, 2010), elimination of hydroxyl and carboxyl groups followed by subsequent aromatization
65 can enhance the drying properties of sludge due to increased hydrophobicity and sludge cell breakage
66 (Wang et al., 2014; Yoshikawa and Prawisudha, 2014a; Zhao et al., 2014b).

67 The drying properties of a material are conveniently characterized through the drying curve where the
68 drying rate is determined as a function of drying time under specific drying conditions. The attained
69 drying curve allows the identification of controlling mechanisms such as moisture evaporation from
70 saturated or unsaturated surfaces or diffusion within a material (Mujumdar, 2007). In addition,
71 effective moisture diffusivity can be used for compiling empiric drying data to a single parameter
72 describing moisture transfer independent of the actual mechanisms involved (Gómez-de la Cruz et al.,
73 2015). Although diffusivity coefficients are often determined through a simplification of Fick's
74 second law of diffusion, reliable estimations for non-rigid materials can only be attained if material
75 shrinkage is taken into account (Bennamoun et al., 2013). Non-extrusive imaging techniques such as
76 X-ray microtomography have been shown to provide detailed quantitative information on material
77 shrinkage and thus enable a better understanding of the relationships between drying properties and
78 the evolution of size and shape (Léonard et al., 2004; Léonard et al., 2008).

79 For reliably determining the effect of hydrothermal treatment on the drying properties of sludge, we
80 illustrate the use of X-ray microtomography for monitoring sample shrinkage during drying of sludge
81 and hydrochar samples. Respective effective moisture diffusivities affected by shrinkage were then
82 determined by applying recent developments on the interpretation of experimental drying data.
83 Finally, the effect and statistical significance of treatment conditions such temperature, retention time
84 and additive quality on the mean moisture diffusivity of hydrochar were determined using multiple
85 linear regression. The attained results help in understanding the effect of process conditions on the
86 drying properties of hydrothermally treated sludge and controlling these properties based on treatment
87 conditions.

88 2. Material and methods

89 2.1 Sampling and sample preparation

90 Sludge samples were attained from a Swedish pulp and paper mill using virgin sulphate and recycled
91 fibre pulp for the production of unbleached kraft/euroliner for corrugated cardboard. Mill effluents
92 were treated by primary gravitational settling followed by biological activated sludge treatment.
93 Approximately 300 kg of mixed sludge (containing 60% of primary sludge and 40% of biosludge)
94 was sampled after primary sludge and surplus biosludge from secondary sedimentation had been
95 mixed and dewatered to approximately 27% dry solids ($2.7 \text{ kg H}_2\text{O kg}^{-1} \text{ db}$, dry basis) using a belt
96 filter and a centrifuge at the mill. The 300 kg sample was coned and quartered (Gerlach et al., 2002)
97 to a representative 10 kg subsample which was stored in $+4 \text{ }^\circ\text{C}$ during the experiments.

98 2.2 Hydrothermal treatment

99 Hydrothermal experiments were performed with a 1 L non-stirred stainless steel reactor (Amar
100 Equipments PVT Ltd., Mumbai, India) illustrated Fig. 1a. A constant 300 g mass of sampled sludge
101 was thoroughly mixed with 75 mL of additive and loaded into the reactor. The reactor was heated to
102 reaction temperature using a 1.5 kW electric heating resistance and an additional heating plate placed
103 under the reactor. The 1.5 kW heating resistance was PID controlled as the additional heating plate
104 was set to reaction temperature. Reactor pressure was indicated by a pressure gauge and was
105 approximately equivalent to saturated vapour pressure of water under respective reaction temperatures
106 (i.e., 1-5 MPa). As the isothermal retention time was complete, the reactor was cooled with
107 pressurized air and the gases released into a fume hood. The solid and liquid phases were
108 subsequently separated by vacuum filtration through a grade 413 VWR® filter paper (VWR
109 International LLC, Radnor, PA, USA).

110 The experiments were conducted according to an experimental design including reaction temperature
111 ($180\text{-}260 \text{ }^\circ\text{C}$) and \log_{10} transformed retention time (0.5-5 h) as continuous controlled variables. In
112 addition, additive type was included as a discrete variable to influence reaction conditions by mixing
113 75 mL NaOH (0.01 N, pH 12.1) or HCl (0.01 N, pH 2.5) with the feed material prior to loading into

114 the reactor. Deionized H₂O was used as a control (conductivity <6 mS cm⁻¹) and both NaOH and HCl
115 used for making the solutions were reagent grade. NaOH was chosen as it is commonly used in the
116 chemical recovery cycles of pulp mills and the inclusion of HCl enabled evaluating the effect of a
117 wider pH range. Additive concentrations were chosen based on Lu et al. (2014) and the final solid
118 load adjusted to remain in the range applicable to dewatered sludge within the pulp and paper
119 industry. As the design included a discrete variable it was constructed to allow the use of dummy
120 variables in linear regression and response surface methodology (Myers et al., 2009). The final design
121 (see Table 1, Section 4) was composed of 15 individual experiments.

122 **Please insert Fig. 1 here**

123 **2.3 Drying experiments and X-ray microtomography**

124 Prior to drying the individual sludge and hydrochar samples were shaped to ensure comparability of
125 initial stress states. The samples were compressed for 1 minute under 50 N in a cylindrical
126 compression cell (Ø 20 mm) consisting of a movable piston and a closed grid that allowed water to be
127 removed. The obtained cylindrical samples were then cut to lengths equivalent to 4.10 ± 0.041 g in
128 sample mass. The corresponding sample volumes were hence dependent on the specific properties of
129 sludge or hydrochar.

130 Drying experiments were performed with a laboratory micro-dryer by following sample mass loss
131 under constant and reproducible drying conditions, Fig. 1b (Léonard et al., 2002). The prepared
132 samples were inserted to a drying chamber (cross-section 41 × 46 mm) on a grid suspended under a
133 precision scale to allow convective drying on the entire external surface. The mass of the samples
134 were then recorded every 5 seconds under an air velocity of 1.5 m s⁻¹, a temperature of 105 °C and an
135 absolute humidity of 0.007 kg H₂O kg⁻¹ dry air. Drying was continued until no further changes in
136 sample mass were observed and the dried samples placed into an oven at 105 °C to determine
137 respective dry solids contents according to standard methods. The mass loss signals were then
138 preprocessed by excluding data points above 95% dry solids (0.053 kg H₂O kg⁻¹ db) for removing
139 interferences at low moisture contents.

140 External surface areas and sample volumes were calculated based on image analysis by X-ray
 141 microtomography. Each sample was scanned before and after drying (Fig. 2) with a 1074 portable X-
 142 ray micro-CT scanner (Skyscan, Kontich, Belgium) for 3 minutes resulting in 105 projections. Each
 143 sample was tilted around 180° recording one projection every 1.7° for minimization of acquisition
 144 time. Sample masses were also measured before and after tomography for linking external surface
 145 areas and sample volumes to respective moisture contents (Fraikin, 2012). Sample shrinkage was
 146 assumed linear in respect to sample moisture contents (Léonard et al., 2004; Li et al., 2014).

147 **Please insert Fig. 2 here**

148 3. Calculations

149 The drying fluxes of sludge and hydrochar samples were calculated by correcting recorded drying
 150 data with the external surface area of each sample from X-ray imaging. In addition, respective sample
 151 volumes were calculated. Raw drying data was also interpreted based on Fick's second law of
 152 diffusion on the hypothesis that moisture transfer is proportional to the concentration gradient of
 153 desorption (Bennamoun et al., 2013):

$$154 \frac{\partial X}{\partial t} = D_{eff,x} \cdot \frac{\partial^2 X}{\partial x^2} + D_{eff,y} \cdot \frac{\partial^2 X}{\partial y^2} + D_{eff,z} \cdot \frac{\partial^2 X}{\partial z^2} \quad (1)$$

155 where X denotes moisture content (kg H₂O kg⁻¹ db), t drying time (s), D_{eff} the effective diffusivity (m²
 156 s⁻¹) and x , y and z the spatial dimensions of moisture transport (m). For short cylinders approaching a
 157 one-dimensional plane sheet with uniform initial moisture distribution Eq. (1) can be expressed as
 158 (Crank, 1975; Pacheco-Aguirre et al., 2014):

$$159 \phi = \frac{X(t) - X_e}{X_0 - X_e} = \frac{8}{\pi^2} \sum_{n=0}^{\infty} \frac{1}{(2n+1)^2} \exp\left(-\frac{(2n+1)^2 \pi^2 D_{eff} t}{L^2}\right) \quad (2)$$

160 where ϕ describes dimensionless moisture ratio, $X(t)$ moisture content (kg H₂O kg⁻¹ db) at time t , X_e
 161 equilibrium moisture content approaching zero on longer drying times, X_0 the initial moisture content,

162 n a positive integer and L sample height (m), i.e. sheet thickness. For considerable drying times Eq.
 163 (2) can be simplified by considering only the first term of the series, which becomes (Crank, 1975):

$$164 \quad \frac{d}{dt} \ln\left(\frac{X(t)}{X_0}\right) = -\frac{D_{eff}\pi^2}{L^2} \quad (3)$$

165 Effective moisture diffusivity can then be determined through:

$$166 \quad D_{eff} = -\frac{kL^2}{\pi^2} \quad (4)$$

167 where k is attained by derivating a polynomial function fitted to the experimental $\ln\left(\frac{X(t)}{X_0}\right)$ data.

168 The effects of controlled design variables, i.e. reaction temperature, retention time and additive
 169 quality, on the effective diffusivities of hydrochar were modelled through a multiple linear regression
 170 equation:

$$171 \quad \mathbf{y} = \mathbf{X}\mathbf{b} + \mathbf{e} \quad (5)$$

172 where \mathbf{y} represents a vector of determined mean diffusivities, \mathbf{X} a coded and range-scaled design
 173 matrix including individual experiments as rows and experimental conditions as the respective
 174 columns, \mathbf{b} a vector of model coefficients and \mathbf{e} a residual vector. Model coefficients were determined
 175 by minimizing the sum of squares of model residuals through the least-squares fit:

$$176 \quad \mathbf{b} = (\mathbf{X}'\mathbf{X})^{-1}\mathbf{X}'\mathbf{y}' \quad (6)$$

177 Individual model coefficients were refined by F-testing the variance explained by a coefficient against
 178 the variance of model residuals calculated as the difference between determined and predicted
 179 diffusivities:

$$180 \quad \mathbf{e} = \mathbf{y} - \hat{\mathbf{y}} \quad (7)$$

181 where $\hat{\mathbf{y}}$ is a vector of predicted mean diffusivities:

$$182 \quad \hat{\mathbf{y}} = \mathbf{X}\mathbf{b} \quad (8)$$

183 The effect of additive quality included as a discrete variable was determined through the use of two
 184 dummy variables c_1 and c_2 in the design matrix \mathbf{X} where:

$$185 \quad c_1 = \begin{cases} 1 & \text{if NaOH is the discrete level} \\ 0 & \text{elsewhere} \end{cases} \quad (9)$$

$$186 \quad c_2 = \begin{cases} 1 & \text{if HCl is the discrete level} \\ 0 & \text{elsewhere} \end{cases} \quad (10)$$

187 The variation of determined diffusivities explained by the model was calculated through the R^2 value:

$$188 \quad R^2 = 1 - \frac{SS_{res}}{SS_{tot}} \quad (11)$$

189 where SS_{res} denotes the sum of squares of model residuals and SS_{tot} the total sum of squares of y
 190 around the mean.

191 **4. Results**

192 A drying time of approximately 80 minutes was required to reach 95% dry solids in the untreated
 193 sludge sample and respectively decreased to a range 37-59 minutes for hydrothermally treated
 194 hydrochar. Time required for drying was accompanied by considerable sample shrinkage especially in
 195 the case of untreated sludge and was inversely correlated with hydrothermal treatment temperature (p
 196 < 0.01) and retention time ($p < 0.01$). The external surface area and volume of sludge and hydrochar
 197 samples assuming linear isotropic shrinkage were attained through X-ray tomography and used for
 198 calculating the drying flux as a function of sample moisture content. The results are provided in Fig.
 199 3a and b.

200 **Please insert Fig. 3 here**

201 The uncorrected drying data were further interpreted based on Fick's second law of diffusion in a one-
 202 dimensional plane sheet. Moisture ratio was first determined as a function of drying time (Fig. 3c) and
 203 the respective natural logarithm fitted with a second order polynomial (Fig. 3d). The attained
 204 polynomial coefficients represented a theoretical fit to the experimental data and were used together

205 with respective sample heights (Fig. 3e) for determining the effective moisture diffusivity of sludge
206 and hydrochar samples (Fig. 3f). As illustrated in Fig. 3f, the determined moisture diffusivities were
207 inversely related to respective moisture contents during drying and thus increased towards the end of
208 the drying experiments. The mean values of determined diffusivities of hydrochar were in the range
209 $12.7\text{-}27.7 \cdot 10^{-9} \text{ m}^2 \text{ s}^{-1}$ (Table 1) and were found statistically different from the moisture diffusivity of
210 untreated sludge ($8.57 \cdot 10^{-9} \text{ m}^2 \text{ s}^{-1}$) on a $p < 0.01$ significance level according to a performed t-test.

211 **Please insert Table 1 here**

212 Coded and range-scaled regression model coefficients for predicting the mean moisture diffusivity of
213 hydrochar were determined and are illustrated in Fig. S1 (Supplementary Information). Both
214 hydrothermal treatment temperature ($p < 0.01$) and transformed retention time ($p < 0.05$) were
215 statistically significant in predicting the mean moisture diffusivity of hydrochar according to the
216 model. No statistically significant relationship was found between mean moisture diffusivity and the
217 dummy variables used for describing additive quality ($p > 0.05$). The F-test performed against model
218 residuals indicated that the attained model was statistically significant on a $p < 0.01$ significance level
219 (Table S1). In addition, the calculated R^2 value suggested that the acquired model explained a
220 satisfactory 76% of variation in the determined mean diffusivities of hydrochar samples.

221 **5. Discussion**

222 As illustrated in Fig. 3a, hydrothermal treatment led to considerable differences in the drying behavior
223 of sludge and hydrochar samples. The drying of untreated sludge began by a short, sharp heating
224 period where the drying flux increased rapidly due to increase in sample temperature. The constant
225 drying rate period generally controlled by vapor transfer at the air-solid interface and the rate of
226 moisture removal could only be seen as a slight increase in drying flux at approximately $2.5 \text{ kg H}_2\text{O}$
227 $\text{kg}^{-1} \text{ db}$ due to simultaneous sample shrinkage (Fig. 3b). On the contrary, drying was mainly governed
228 by the falling rate period during which the drying flux decreased continuously with a decrease in
229 sludge moisture content. This period likely began as surface moisture was sufficiently reduced and

230 moisture was transported to the surface of the solid by capillary forces (Bennamoun et al., 2013;
231 Mujumdar, 2007). Moisture diffusion caused by concentration gradients within the sample matrix and
232 heat conduction are generally regarded as the controlling mechanisms (Léonard et al., 2002).

233 In the case of hydrochar the initial moisture contents were lower due to the hydrothermal treatment
234 and subsequent solid-liquid separation by filtering. Hydrothermal treatment increased the drying flux
235 of hydrochar and respectively decreased the length of the falling rate period (Fig. 3a) most likely due
236 to sludge cell breakage (Dawei et al., 2012). In addition, two different phases could be observed
237 during the falling rate period, the phases being especially distinguishable at approximately 0.5 kg H₂O
238 kg⁻¹ db for samples treated at 260 °C. As discussed by Léonard et al. (2002), the first phase of the
239 falling rate period is normally governed by decreasing drying air humidity at the air-solid interface
240 due to heat and mass transfer limitations and simultaneous sample shrinkage. During the second phase
241 sample shrinkage decreases or ceases entirely as the decreasing drying flux is almost entirely caused
242 by internal heat and mass transfer limitations (Léonard et al., 2002). Our observations on sample
243 shrinkage in Fig. 3b do not entirely support this description as they assume linear isotropic shrinkage
244 measured before and after the drying experiments. However, it is more likely that a higher degree of
245 shrinkage occurred in the beginning of the drying process during the constant rate period and the first
246 phase of the falling rate period (Fig. 3a) especially with hydrochar samples where different falling rate
247 periods could be distinguished. As illustrated in Fig. 3b hydrothermal treatment decreased sample
248 shrinkage and the effect of heat and mass transfer limitations based on an increased drying flux.

249 Moisture diffusivity coefficients are often determined based on a simplification of Fick's second law
250 of diffusion assuming isotropic diffusion (Pacheco-Aguirre et al., 2014). As illustrated in Fig. 3f, the
251 determined effective moisture diffusivities of sludge and hydrochar increased as a function of
252 decreasing moisture content. As described by Fyhr and Kemp (1998), moisture diffusivity in solids is
253 nearly constant at higher moisture contents but generally reaches a peak when no free moisture is left
254 in the solid and the only remaining mechanisms for moisture transport are diffusion and convective
255 vapour flow. However, the peak is generally followed by a notable decrease in diffusivity as the
256 moisture content of the solid approaches zero. In our data the determined diffusivities turned towards

257 zero at low moisture contents, but could not be observed in Fig. 3f as the drying data was
258 preprocessed by excluding data points beyond 95% dry solids. This affected the coefficients attained
259 by fitting a polynomial function to the experimental data, but ensured comparability of mean moisture
260 diffusivities between different samples. Recently Gómez-de la Cruz et al. (2015) reported a
261 modification for the determination of effective diffusivities by using a second order polynomial for
262 describing moisture ratio as a function of time. The authors also showed increasing effective
263 diffusivities as a function of decreasing moisture contents and increasing drying temperature for rigid
264 olive stone. In our case the modification yielded R^2 values in the range 0.996-0.999 for sludge and
265 hydrochar samples and was hence adopted (Fig. 3d). This method also allowed taking sample
266 shrinkage into account by including a time dependent function for sample height. As illustrated in Fig.
267 3b and e considerable sample shrinkage occurred especially with untreated sludge and hydrochar from
268 lower treatment temperatures. Shrinkage however decreased considerably with an increase in
269 hydrothermal treatment temperature, which also increased effective diffusivity of hydrochar at lower
270 moisture contents (Fig. 3f). Previously Zhao et al. (2014a) investigated the drying properties of
271 hydrothermally treated paper sludge and reported effective diffusivities in the range $1.26-1.71 \cdot 10^{-9}$
272 $\text{m}^2 \text{s}^{-1}$ for hydrochar treated at 180-260 °C for 30 minutes. The authors used drying temperatures of 30
273 °C, did not take shrinkage into account and used a linear model for describing the evolution of
274 moisture ratio as a function of drying time. However, Bennamoun et al. (2013) reported a diffusivity
275 difference of 106-134% if shrinkage is not taken into account during laboratory drying experiments
276 on municipal sludge.

277 The attained regression model indicated that hydrothermal treatment temperature was 1.6 times as
278 important as transformed retention time in controlling the mean moisture diffusivity of hydrochar
279 (Fig. S1). As the experimental variables were coded and range-scaled their effects could be compared
280 within the original design range. In addition, the dummy variables used for describing the effect of
281 acid and base additions suggested that the use of NaOH or HCl did not significantly affect the mean
282 moisture diffusivity of hydrochar ($p > 0.05$). Previously the effect of process conditions have mainly
283 been investigated in terms of solid fuel properties and yields of attained hydrochar. Although it is

284 currently well known that temperature mainly governs biomass decomposition in hydrothermal
285 media, retention time has also been found significant for the fuel properties of hydrochar produced
286 from algae and municipal and industrial sludge (Danso-Boateng et al., 2015; Heilmann et al., 2011;
287 Mäkelä et al., 2015; Xu et al., 2013). In addition, Lynam et al. (2011) found that organic acid
288 additions enhanced cellulose dissolution and respectively decreased hydrochar yield during
289 hydrothermal treatment of lignocellulosic biomass. Furthermore, Lu et al. (2014) reported statistically
290 different solid yields of hydrothermally treated cellulose in NaOH and HCl due to changes in reaction
291 kinetics. In this work the mean diffusivities of hydrochar were higher with the use of H₂O than with
292 NaOH or HCl, but the overall differences were not statistically significant (Fig. S1). Liquid pH values
293 measured after the hydrothermal experiments were in the range 4.9-5.5 and correlated only with
294 treatment temperature ($p < 0.01$) and retention time ($p < 0.05$). This suggests that the strength of used
295 additives were not sufficient to significantly change reaction conditions and were neutralized likely
296 due to the formation of organic acids during biomass decomposition under hydrothermal conditions
297 (Berge et al., 2011; Weiner et al., 2014). Equivalent hydroxide and hydronium ion concentrations
298 from NaOH and HCl have previously been used for simulating different pH environments in
299 municipal and industrial waste streams (Lu et al., 2014). In addition, equivalent hydroxide
300 concentrations from KOH have been reported to lead to decreased surface area and pore volume of
301 hydrothermally treated wheat straw (Reza et al., 2015) which could have practical implications for the
302 drying behavior of hydrochar. Besides evaluating the effect of process conditions the attained model
303 coefficients enable prediction of novel observations, which is very useful for illustrating the behavior
304 of mean diffusivity of hydrochar within the design range. Respective contours were hence calculated
305 based on hydrothermal treatment temperature and retention time in NaOH, H₂O and HCl and are
306 shown in Fig. 4. The linear increase in mean diffusivity as a function reaction temperature and
307 retention time could easily be observed and was more pronounced with NaOH or H₂O compared to
308 HCl. As an example, hydrothermal treatment at 220 °C with a retention time of 1.5 h in H₂O would be
309 expected to increase the mean effective diffusivity of sludge to $18.2 \pm 5.80 \cdot 10^{-9} \text{ m}^2 \text{ s}^{-1}$ with 95%
310 certainty. According to our better knowledge this is the first time the effect and statistical significance
311 of hydrothermal treatment conditions on the mean moisture diffusivity and drying behavior of sludge

312 have been reported. Once these effects are known, the mean diffusivity of sludge can be predicted
313 within the design thus allowing control of respective drying properties based on hydrothermal
314 treatment conditions. This information is vital for optimizing hydrothermal treatment and subsequent
315 drying processes for this feedstock.

316 **Please insert Fig. 4 here**

317 **Conclusions**

318 Hydrothermal treatment enhanced the drying properties and increased the effective moisture
319 diffusivity of sludge. Drying of untreated sludge was governed by the falling rate period where drying
320 flux decreased continuously as a function of sludge moisture content due to heat and mass transfer
321 limitations and sample shrinkage. Hydrothermal treatment increased the drying flux of sludge
322 hydrochar and decreased the effect of internal heat and mass transfer limitations and sample shrinkage
323 especially at higher treatment temperatures. The determined effective moisture diffusivities increased
324 as a function of decreasing moisture content and a statistically significant difference was found
325 between the mean diffusivity of untreated sludge and sludge hydrochar. The attained regression model
326 indicated that treatment temperature controlled the mean moisture diffusivity of hydrochar as the
327 effects of NaOH and HCl were found statistically insignificant. The presented results enabled
328 prediction of sludge drying properties through mean moisture diffusivity based on hydrothermal
329 treatment conditions.

330 **Acknowledgements**

331 The contributions of Markus Segerström and Gunnar Kalén from the Swedish University of
332 Agricultural Sciences in sample processing are deeply appreciated. This work was performed in
333 cooperation with SCA Obbola AB with partial funding from SP Processum AB.

334 **References**

- 335 Alatalo, S.-M., Repo, E., Mäkilä, E., Salonen, J., Vakkilainen, E., Sillanpää, M., 2013. Adsorption
336 behavior of hydrothermally treated municipal sludge & pulp and paper industry sludge. *Bioresource*
337 *Technology* 147, 71-76. doi: 10.1016/j.biortech.2013.08.034.
- 338 Bennamoun, L., Crine, M., Léonard, A., 2013. Convective drying of wastewater sludge: introduction
339 of shrinkage effect in mathematical modeling. *Drying Technology* 31, 643-654. doi:
340 10.1080/07373937.2012.752743.
- 341 Berge, N.D., Ro, K.S., Mao, J., Flora, J.R.V., Chappell, M.A., Bae, S., 2011. Hydrothermal
342 carbonization of municipal waste streams. *Environmental Science and Technology* 45, 5696-5703.
343 doi: 10.1021/es2004528.
- 344 Crank, J. *The Mathematics of Diffusion* (2nd ed.). Oxford University Press: London, 1975, 414 pp.
- 345 Danso-Boateng, E., Shama, G., Wheatley, A.D., Martin, S.J., Holdich, R.G., 2015. Hydrothermal
346 carbonisation of sewage sludge: effect of process conditions on product characteristics and methane
347 production. *Bioresource Technology* 177, 318-327. doi: 10.1016/j.biortech.2014.11.096.
- 348 Dawei, M., Zili, J., Yoshikawa, K., Hongyan, M., 2012. The effect of operation parameters on the
349 hydrothermal drying treatment. *Renewable Energy* 42, 90-94. doi: 10.1016/j.renene.2011.09.011.
- 350 Fraikin, L., Contribution à l'étude du séchage convectif de boues de station d'épuration et des
351 émissions gazeuses associées, University of Liège, Department of Chemical Engineering, 2012.
- 352 Fyhr, C., Kemp, I.C., 1998. Comparison of different drying kinetics models for single particles.
353 *Drying Technology* 16, 1339-1369. doi: 10.1080/07373939808917465.
- 354 Gerlach, R.W., Dobb, D.E., Raab, G.A., Nocerino, J.M., 2002. Gy sampling theory in environmental
355 studies. 1. Assessing soil splitting protocols. *Journal of Chemometrics* 16, 321-328. doi:
356 10.1002/cem.705.

- 357 Gómez-de la Cruz, F.J., Palomar-Carnicero, J.M., Casanova-Peláez, P.J., Cruz-Peragón, F., 2015.
358 Experimental determination of effective moisture diffusivity during the drying of clean olive stone:
359 dependence of temperature, moisture content and sample thickness. *Fuel Processing Technology* 137,
360 320-326. doi: 10.1016/j.fuproc.2015.03.018.
- 361 Heilmann, S.M., Jader, L.R., Sadowsky, M.J., Schendel, F.J., von Keitz, M.G., Valentas, K.J., 2011.
362 Hydrothermal carbonization of distiller's grains. *Biomass and Bioenergy* 35, 2526-2533. doi:
363 10.1016/j.biombioe.2011.02.022.
- 364 Kruse, A., Funke, A., Titirici, M.-M., 2013. Hydrothermal conversion of biomass to fuels and
365 energetic materials. *Current Opinion in Chemical Biology* 17, 515-521. doi:
366 10.1016/j.cbpa.2013.05.004.
- 367 Léonard, A., Blacher, S., Marchot, P., Crine, M., 2002. Use of X-ray microtomography to follow the
368 convective heat drying of wastewater sludges. *Drying Technology* 20, 1053-1069. doi: 10.1081/DRT-
369 120004013.
- 370 Léonard, A., Blacher, S., Marchot, P., Pirard, J.P., Crine, M., 2004. Measurement of shrinkage and
371 cracks associated to convective drying of soft materials by X-ray microtomography. *Drying*
372 *Technology* 22, 1695-1708. doi: 10.1081/DRT-200025629.
- 373 Léonard, A., Meneses, E., Le Trong, E., Salmon, T., Marchot, P., Toye, D., Crine, M., 2008.
374 Influence of back mixing on the convective drying of residual sludges in a fixed bed. *Water Research*
375 42, 2671-2677. doi: 10.1016/j.watres.2008.01.020.
- 376 Li, J., Bennamoun, L., Fraikin, L., Salmon, T., Toye, D., Schreinemachers, R., Léonard, A., 2014.
377 Analysis of the shrinkage effect on mass transfer during convective drying of sawdust/sludge
378 mixtures. *Drying Technology* 32, 1706-1717. doi: 10.1080/07373937.2014.924136.
- 379 Libra, J.A., Ro, K.S., Kammann, C., Funke, A., Berge, N.D., Neubauer, Y., Titirici, M.-M., Fühner,
380 C., Bens, O., Kern, J., Emmerich, K.-H., 2011. Hydrothermal carbonization of biomass residuals: a

- 381 comparative review of the chemistry, processes and applications of wet and dry pyrolysis. *Biofuels* 2,
382 71-106. doi: 10.4155/BFS.10.81.
- 383 Lu, X., Flora, J.R.V., Berge, N.D., 2014. Influence of process water quality on hydrothermal
384 carbonization of cellulose. *Bioresource Technology* 154, 229-239. doi:
385 10.1016/j.biortech.2013.11.069.
- 386 Lynam, J.G., Coronella, C.J., Yan, W., Reza, M.T., Vasquez, V.R., 2011. Acetic acid and lithium
387 chloride effects on hydrothermal carbonization of lignocellulosic biomass. *Bioresource Technology*
388 102, 6192-6199. doi: 10.1016/j.biortech.2011.02.035.
- 389 Mahmood, T., Elliott, A., 2006. A review of secondary sludge reduction technologies for the pulp and
390 paper industry. *Water Research* 40, 2093-2112. doi: 10.1016/j.watres.2006.04.001.
- 391 Mäkelä, M., Benavente, V., Fullana, A., 2015. Hydrothermal carbonization of lignocellulosic
392 biomass: effect of process conditions on hydrochar properties. *Applied Energy* 155, 576-584. doi:
393 10.1016/j.apenergy.2015.06.022.
- 394 Mowla, D., Tran, H.N., Grant Allen, D., 2013. A review of the properties of biosludge and its
395 relevance to enhanced dewatering processes. *Biomass and Bioenergy* 58, 365-378. doi:
396 10.1016/j.biombioe.2013.09.002.
- 397 Mujumdar, A.S., Principles, Classification and Selection of Dryers. In: *Handbook of Industrial Drying*
398 (3rd ed.), A. S. Mujumdar (Eds.), CRC Press: Boca Raton; 2007, pp. 4-32.
- 399 Myers, R.H., Montgomery, D.C., Anderson-Cook, C.M., Experimental Designs for Fitting Response
400 Surfaces - II. In: *Response Surface Methodology: Process and Product Optimization Using Designed*
401 *Experiments* (3rd ed.), R. H. Myers, D. C. Montgomery and C. M. Anderson-Cook (Eds.), John Wiley
402 & Sons, Inc.: Hoboken; 2009, pp. 349-416.

- 403 Pacheco-Aguirre, F.M., Ladrón-González, A., Ruiz-Espinosa H, García-Alvarado, M.A., Ruiz-López,
404 I.I., 2014. A method to estimate anisotropic diffusion coefficients in cylindrical solids: application to
405 the drying of carrot. *Journal of Food Engineering* 125, 24-33. doi: 10.1016/j.jfoodeng.2013.10.015.
- 406 Peterson, A.A., Vogel, F., Lachance, R.P., Fröling, M., Antal Jr., M.M., Tester, J.W., 2008.
407 Thermochemical biofuel production in hydrothermal media: a review of sub- and supercritical water
408 technologies. *Energy & Environmental Science* 1, 32-65. doi: 10.1039/b810100k.
- 409 Reza, M.T., Rottler, E., Herklotz, L., Wirth, B., 2015. Hydrothermal carbonization (HTC) of wheat
410 straw: influence of feedwater pH prepared by acetic acid and potassium hydroxide. *Bioresource*
411 *Technology* 182, 336-344. doi: 10.1016/j.biortech.2015.02.024.
- 412 Sevilla, M., Fuertes, A.B., 2009. The production of carbon materials by hydrothermal carbonization
413 of cellulose. *Carbon* 47, 2281-2289. doi: 10.1016/j.carbon.2009.04.026.
- 414 Stoica, A., Sandberg, M., Holby, O., 2009. Energy use and recovery strategies within wastewater
415 treatment and sludge handling at pulp and paper mills. *Bioresource Technology* 100, 3497-3505. doi:
416 10.1016/j.biortech.2009.02.041.
- 417 Titirici, M.-M., Antonietti, M., 2010. Chemistry and material options of sustainable carbon materials
418 made by hydrothermal carbonization. *Chemical Society Reviews* 39, 103-116. doi:
419 10.1039/b819318p.
- 420 Vaxelaire, J., Cézac, P., 2004. Moisture distribution in activated sludges: a review. *Water Research*
421 38, 2215-2230. doi: 10.1016/j.watres.2004.02.021.
- 422 Wang, L., Zhang, L., Li, A., 2014. Hydrothermal treatment coupled with mechanical expression at
423 increased temperature for excess sludge dewatering: influence of operating conditions and process
424 energetics. *Water Research* 65, 85-97. doi: 10.1016/j.watres.2014.07.020.

- 425 Weiner, B., Poerschmann, J., Wedwitschka, H., Koehler, R., Kopinke, F.-D., 2014. Influence of
426 process water reuse on the hydrothermal carbonization of paper. *ACS Sustainable Chemistry &*
427 *Engineering* 2, 2165-2171. doi: 10.1021/sc500348v.
- 428 Xu, Q., Qian, Q., Quek, A., Ai, N., Zeng, G., Wang, J., 2013. Hydrothermal carbonization of
429 macroalgae and the effects of experimental parameters on the properties of hydrochars. *ACS*
430 *Sustainable Chemistry & Engineering* 1, 1092-1101. doi: 10.1021/sc400118f.
- 431 Yoshikawa, K., Prawisudha, P., Hydrothermal Treatment of Municipal Solid Waste for Producing
432 Solid Fuel. In: *Application of Hydrothermal Reactions to Biomass Conversion* (1st ed.), F. Jin (Eds.),
433 Springer: Heidelberg; 2014a, pp. 355-383.
- 434 Yoshikawa, K., Prawisudha, P., Sewage Sludge Treatment by Hydrothermal Process for Producing
435 Solid Fuel. In: *Application of Hydrothermal Reactions to Biomass Conversion* (1st ed.), F. Jin (Eds.),
436 Springer: Heidelberg; 2014b, pp. 385-409.
- 437 Zhao, P., Ge, S., Ma, D., Areeprasert, C., Yoshikawa, K., 2014a. Effect of hydrothermal pretreatment
438 on convective drying characteristics of paper sludge. *ACS Sustainable Chemistry & Engineering* 2,
439 665-671. doi: 10.1021/sc4003505.
- 440 Zhao, P., Shen, G., Ge, S., Chen, Z., Yoshikawa, K., 2014b. Clean solid biofuel production from high
441 moisture content waste biomass employing hydrothermal treatment. *Applied Energy* 131, 345-367.
442 doi: 10.1016/j.apenergy.2014.06.038.
- 443

Table 1: Hydrothermal carbonization conditions and calculated effective moisture diffusivities of hydrochar.

Exp. n:o	Reaction temperature (°C)	Retention time		Catalyst	Determined mean effective diffusivity ($10^{-9} \text{ m}^2 \text{ s}^{-1}$) ^a
		h	log ₁₀ h		
1	180	0.50	-0.3	NaOH	12.7
2	260	0.50	-0.3	NaOH	17.9
3	180	5.00	0.699	NaOH	13.9
4	260	5.00	0.699	NaOH	27.5
5	180	1.58	0.1995	NaOH	13.6
6	220	5.00	0.699	NaOH	18.1
7	180	0.50	-0.3	H ₂ O	14.8
8	260	0.50	-0.3	H ₂ O	18.2
9	180	5.00	0.699	H ₂ O	16.4
10	260	5.00	0.699	H ₂ O	23.8
11	180	0.50	-0.3	HCl	13.2
12	260	0.50	-0.3	HCl	16.7
13	180	5.00	0.699	HCl	17.0
14	260	5.00	0.699	HCl	18.9
15	220	1.58	0.1995	HCl	14.7

^a Mean effective moisture diffusivity of untreated sludge $8.56 \cdot 10^{-9} \text{ m}^2 \text{ s}^{-1}$

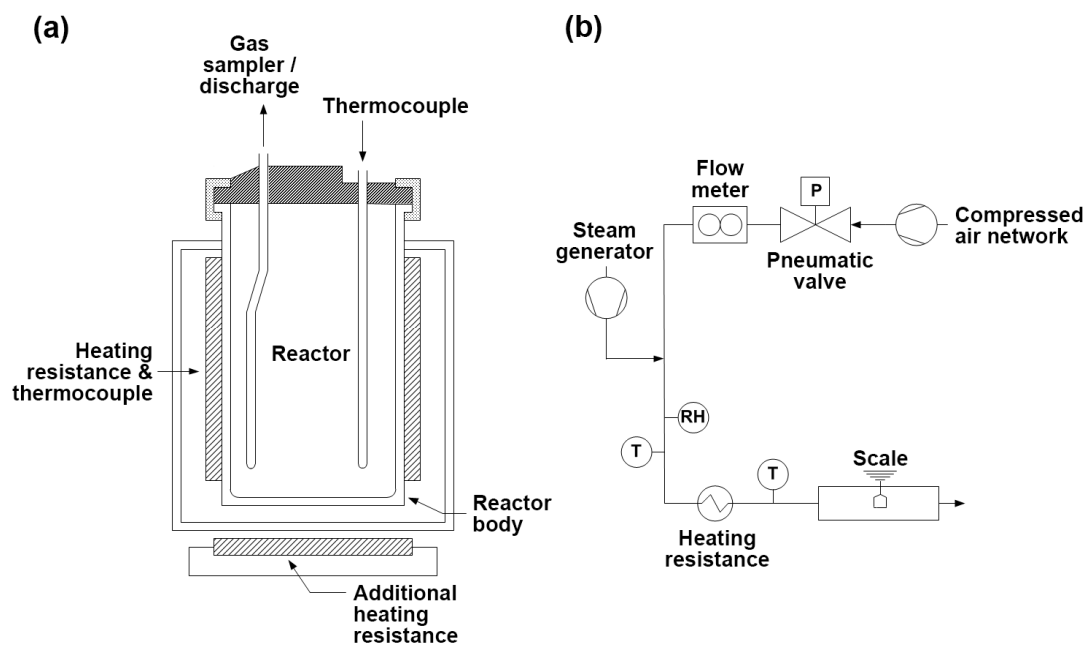


Fig. 1: Schematic presentations of a) the hydrothermal reactor and b) the microdryer.

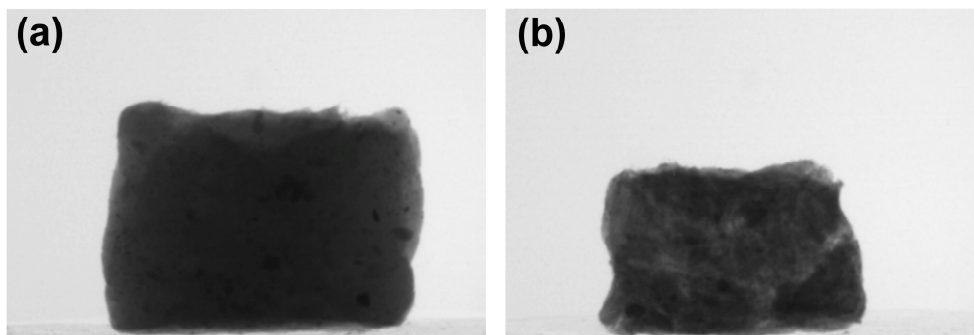


Fig. 2: Example X-ray images of untreated mixed sludge a) before and b) after drying.

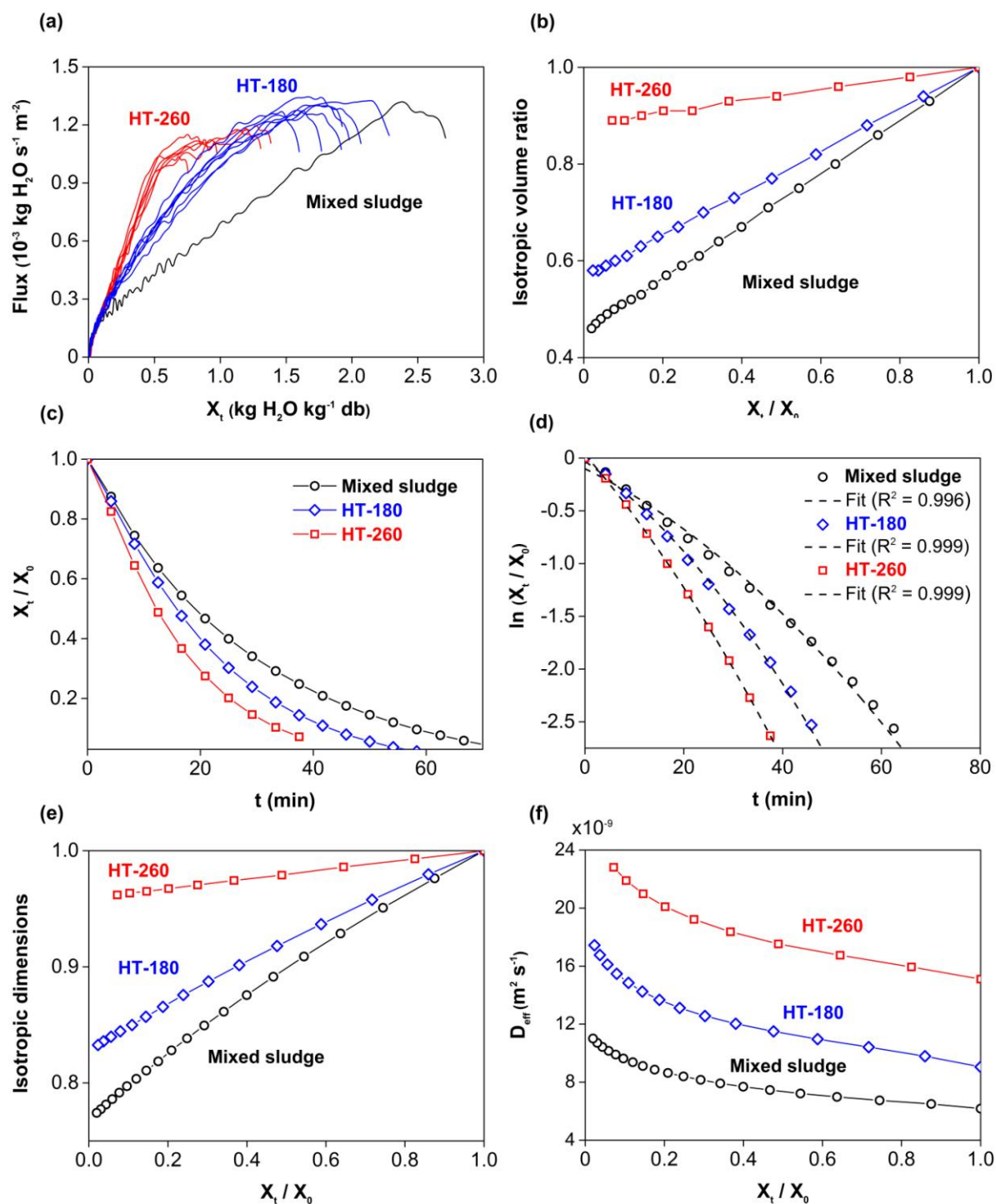


Fig. 3: a) Drying flux; b) Isotropic volume ratios; c) Moisture ratios (X_t / X_0); d) Polynomial fit of $\ln(X_t / X_0)$; e) Isotropic dimension ratios; and f) Effective moisture diffusivities ($10^{-9} \text{ m}^2 \text{ s}^{-1}$) of sludge and hydrochar as a function of moisture ratio. In a) only hydrochar samples produced at 180 and 260 °C and in b)-f) only three samples (untreated sludge and exp. no. 11 and 14, Table 1) and every 50th data point are shown for clarity. The color version is available in the online version.

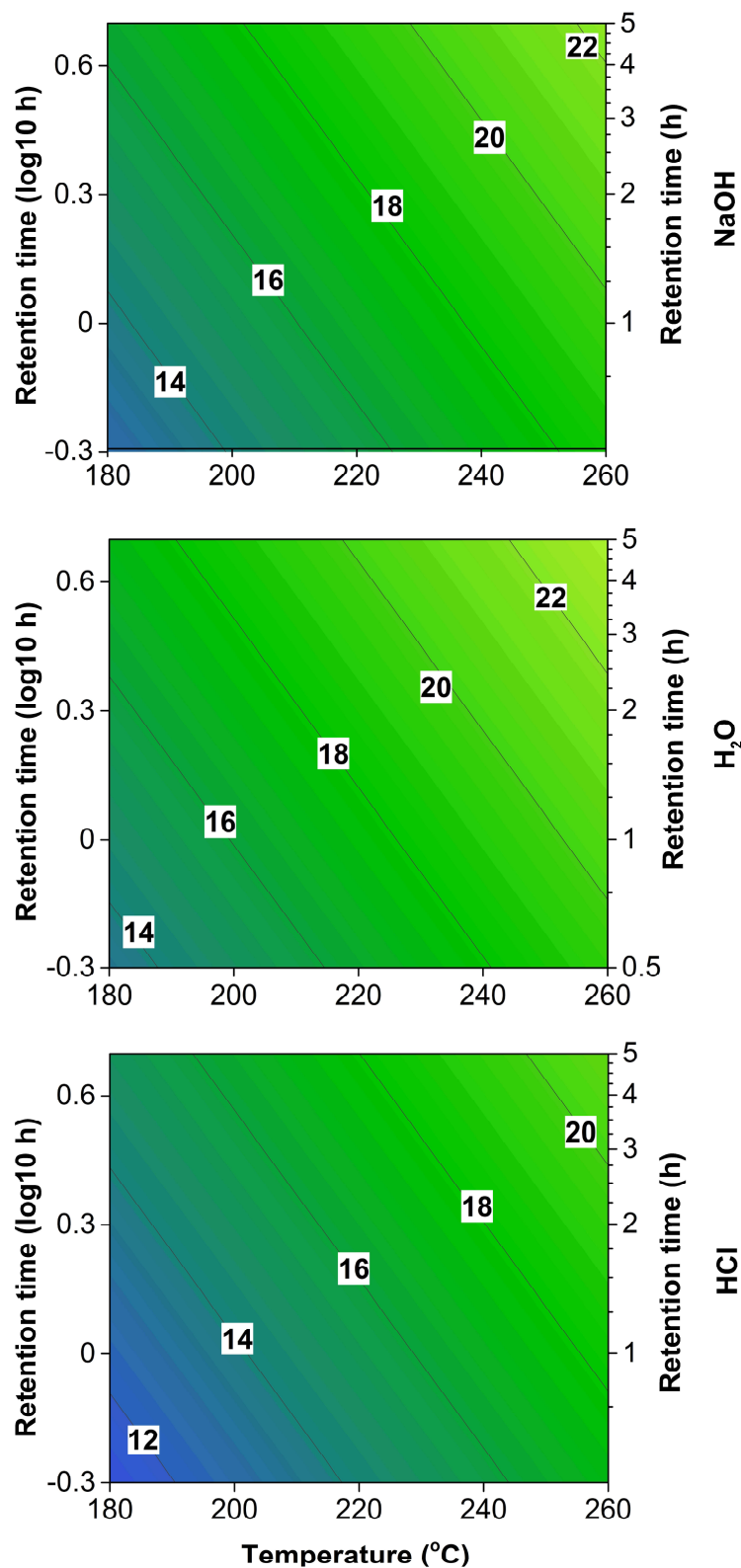


Fig. 4: Predicted mean effective moisture diffusivity ($10^{-9} \text{ m}^2 \text{ s}^{-1}$) of hydrochar as a function of reaction temperature ($^{\circ}\text{C}$) and retention time (h) in NaOH, H₂O and HCl. *The color version is available in the online version.*

Highlights

- Hydrothermal treatment increased drying flux and decreased sludge shrinkage
- Effective moisture diffusivity increased as a function of decreasing sample moisture
- Treatment temperature controlled the mean diffusivity of sludge hydrochar
- Drying properties predicted based on hydrothermal treatment conditions